Radiation Science and Technology
2022; 8(2): 30-37
http://www.sciencepublishinggroup.com/j/rst
doi: 10.11648/j.rst.20220802.12
ISSN: 2575-5935 (Print); ISSN: 2575-5943 (Online)

Commissioning Experience of a Medical Linear Accelerator in a Low-Resource Setting in Sub-Saharan Africa

Paul Njom Mobit[1, 2], Nicholas Ade[1, 2, *]

[1]Department of Radiation Oncology, Cameroon Oncology Center, Douala, Cameroon

[2]Cameroon Cancer Foundation, Douala, Cameroon

Email address:

mobit_paul@yahoo.ca (P. N. Mobit), nickade00@yahoo.com (N. Ade)

[*]Corresponding author

To cite this article:

Paul Njom Mobit, Nicholas Ade. Commissioning Experience of a Medical Linear Accelerator in a Low-Resource Setting in Sub-Saharan Africa. *Radiation Science and Technology*. Vol. 8, No. 2, 2022, pp. 30-37. doi: 10.11648/j.rst.20220802.12

Received: May 5, 2022; **Accepted**: May 28, 2022; **Published**: June 9, 2022

Abstract: With increasing cancer incidence in Africa, a number of Sub-Saharan African countries have started implementing radiotherapy programs based on linear accelerator (linac) technology. This work summarizes the commissioning experience of a commercially available medical linac installed in a resource-limited oncology centre in Cameroon for the delivery of high-quality radiation treatments to cancer patients in central Africa. Cameroon is a central African country in Sub-Saharan Africa. Using a 2D water phantom and various ionization chambers, we measured commissioning data for a medical linac with 6X and 18X photon beams, and five electron energies ranging from 6–20 MeV. Relative measurements included percent depth doses (PDDs), beam profiles, scatter factors, wedge factors, and electron cone factors. Absolute calibrations of the beam energies were performed using the American Association of Physicist in Medicine Task Group Report 51. Accurate calibrations were checked by irradiating the mailed thermoluminescent dosimeters service offered by MD Anderson Cancer Center. Photon PDDs agreed within 1% of the average of several linacs of the same type at depths between 5 and 20 cm, which are consistent with the data used by the manufacturer for acceptance testing. For electrons, the agreement was within 2 mm for R_{50}, R_{90}, R_p, and d_{max}. Symmetry and flatness for all photon and electron beams were within 2% for various fields. All absolute calibrations met the MD Anderson Cancer Center criteria within 3%. This work presents the successful implementation and modernization of a radiotherapy program based on linac technology in the central African sub-region in Sub-Saharan Africa. As the first operational medical linac in the sub-region, the commissioning data can provide comparison data to other linacs in the future to ensure high-quality of machine commissioning for clinical use.

Keywords: Radiotherapy, Medical Linac, Commissioning Experience, Cameroon Oncology Center

1. Introduction

Cancer is a growing health concern worldwide affecting more people in developing countries than in the developed economies [1]. The incidence of cancer is escalating, predominantly because of the increase in life expectancies arising from worldwide improvements in standards of living [2]. Currently, cancer ranks as one of the leading causes of death in the world [3, 4]. It is estimated that one in three people will develop cancer during their lifetime [5]. According to recent estimates of the International Agency for Research (IARC) on cancer employing statistics from GLOBOCAN (the Global Cancer Incidence, Mortality and Prevalence) database, the global cancer burden is estimated to have increased to 19.3 million new cases and 10.0 million deaths in 2020 [3, 6, 7]. This increase is a 9.4% growth from the 2018 estimate of 18.1 million cases [8, 9]. GLOBOCAN 2020 report predicted further that countries classified as low or medium Human Development Index (the developing or low-to-middle-income countries) will have the largest relative cancer incidence by 2040 (a 95% and 64% projected increase from 2020, respectively). These developing countries are known to have weak health infrastructure, and sparse cancer services to deal with this dramatic increase in the number of cases [9]. Remarkably, GLOBOCAN 2020 figures show a cancer incidence of nearly 1.1 million new cases per year, with about 711,000 deaths (64.1% deaths

relative to incidence) in Africa, compared to the world statistics of 19.3 million cancer cases and 10 million deaths (51.8% deaths relative to incidence). In Sub-Saharan Africa (SSA) alone, the estimated number of new cancer cases in 2020 was 801,392 with 520,158 deaths. With an estimated 28.4 million new cancer cases expected to occur in 2040, a 47% increase relative to 2020, Sub-Saharan African countries might not be prepared to handle the burden if resource-appropriate cancer control programs are not accelerated as a matter of urgency. Therefore, countries in SSA must develop policies that would lead to commissioning of many more cancer diagnosing and treatment centers.

Radiation therapy or radiotherapy (RT), a key component of cancer control programs uses ionizing radiation for the treatment of cancer. Its goal is to deliver a lethal radiation dose into the tumour while maximally sparing nearby healthy tissues and organs, thereby leading to a better treatment outcome for the patient. Modern external beam radiation therapy (EBRT) employs megavoltage electrons (6–22 MeV) or x-ray photons (4–25 MV) produced by medical linear accelerators (linacs). If the number of teletherapy machines per million people is used as an indicator for access to RT in a given region, then SSA is known to have sparse RT facilities, with an average capacity of less than one teletherapy machine per million people [10]. An analysis of RT machines in Africa using information from the International Atomic Energy Agency's (IAEA) Directory of Radiotherapy Centres (DIRAC) database in 2010 showed that majority of RT facilities are concentrated in North Africa and Southern Africa, with South Africa and Egypt alone accounting for about 60% of the RT resources [10]. These statistics thus highlight the disparity situation in other parts of SSA. For instance, by the end of March 2019, Cameroon, a country in central Africa had only one functioning Cobalt-60 teletherapy unit serving a population of about 26 million people.

One major challenge that has hindered the development of RT facilities in SSA is that RT is capital intensive and requires skilled personnel that take years to train. However, since most cancers diagnosed in resource-scarce countries like those in SSA are diagnosed at advanced stages, and estimates are that more than half of all cancer patients will require RT in the management of their cancers [1, 11]. The requirements for RT services in SSA are becoming bigger. To lessen the impact of cancer in SSA, Cameroon Oncology Center (COC), a resource-limited oncology centre in Central Africa recently implemented a RT program based on medical linac technology. The purpose of this paper is to share the commissioning experience of the commercially available medical linac installed at COC. Cameroon Oncology Center is located on the outskirts of the metropolis of Douala in the Littoral Region of Cameroon. It is a revenue neutral private oncology centre that treats cancer patients from all over Cameroon and all the six neighbouring countries including Nigeria and Congo-Kinshasa. The centre also has an outpatient chemotherapy infusion room with eight chairs and twenty private room suites for hospitalization. The first radiotherapy patient received radiation treatment on April 1st, 2019.

2. Methods and Materials

A commercially available Clinac 21EX linac (Varian Medical Systems, Palo Alto, CA) with 6 MV and 18 MV photons, and five electron energies ranging from 6–20 MeV was commissioned. It is equipped with a dynamic wedge, 120 Millennium MLCs (comprising two opposing leaf banks with leaves that move along the X-axis), and a Portal Imager AS500 for correct patient setup. One of the objectives of commissioning a medical linac is to collect data so that monitor units (MU) can be determined for each treatment field. This was traditionally used for hand calculations before the coming of computerized second-check MU verification systems such as RADCALC™ (https://www.lifelinesoftware.com) or MUCheck™ (https://mucheck.com/odshome/). Another objective of medical linac commissioning is to collect data for the commissioning of a radiation treatment planning system (TPS), which is not addressed in this manuscript. The MU for photon beams can be obtained from:

$$\mathrm{MU}=\frac{\mathrm{DFD}}{F_{\mathrm{cal}}\times \mathrm{TPR}(\mathrm{d},F_{\mathrm{eff}})\times S_c(X\times Y)\times S_p(F_{\mathrm{eff}})\times F_{\mathrm{block}}\times \mathrm{OAF}\times \mathrm{WF}\times I_{\mathrm{prescription}}\times \mathrm{SSD}_{\mathrm{factor}}} \quad (1)$$

where, *MU* is the number of monitor units required to deliver the daily field dose, *DFD*; $Fcal$ is the cGy/MU calibration factor. It takes into account the fact that the machine is calibrated using an SSD (source-to-surface distance) setup and patient calculations are done using an isocentric or SAD (source-to-axis distance) setup; *TPR (d, F_{eff})* is the tissue phantom ratio at a depth *d* for the equivalent field, F_{eff}. $S_c(X \times Y)$ is the collimator scatter factor for the given X × Y field or equivalent field size; $S_p(F_{\mathrm{eff}})$ is the phantom scatter factor of an effective field size, F_{eff} (relative to a 10 × 10 cm^2 open field); F_{block} is the block or tray factor; OAF(r,d) is the off-axis factor for a radius *r* cm and depth *d*; $I_{\mathrm{prescription}}$ is the prescription isodose line/100; *WF* is the wedge factor, defined as: $WF=WTF\times WFS\times HCF\times WOAF$; where, *WTF* is the wedge transmission factor (measured for 10 × 10 cm^2 field size), *WFS* is the wedge field size factor (relative to 10 × 10 cm^2 field), *HCF* is the hardening correction factor. It is a function of depth for a 10 ×10 cm^2 field, and *WOAF* is the wedge off-axis factor.

$$\mathrm{SSD}_{\mathrm{factor}}=\left(\frac{100.0}{\mathrm{SSD}_{\mathrm{patient}}+\mathrm{depth}_{\mathrm{patient}}}\right)^2 \quad (2)$$

where, $\mathrm{SSD}_{\mathrm{patient}}$ and $\mathrm{depth}_{\mathrm{patient}}$ are the patient SSD and depth, respectively.

For electron beams, the MU can be calculated from:

$$\mathrm{MU}=\frac{\mathrm{DFD}}{F_{\mathrm{cal}}\times \mathrm{RCF}\times \mathrm{ICF}(F_{\mathrm{eff}})\times I_{\mathrm{prescription}}\times \mathrm{SSD}_{\mathrm{factor}}} \quad (3)$$

Where, *RCF* is the relative cone factor, *ICF* is the insert correction factor, and

$$\mathrm{SSD_{factor}} = \left(\frac{\mathrm{SSD_{virtual}} + \mathrm{d_{ref}}}{\mathrm{SSD_{patient}} + \mathrm{depth_{patient}}}\right)^2 \quad (4)$$

Where, $\mathrm{SSD_{virtual}}$ is the virtual SSD, and d_{ref} is the reference calibration depth.

The process of acceptance testing and commissioning a medical linac requires the purchase of additional equipment. The commissioning process can take up a considerable amount of time, effort, and in a resource-limited environment with no prior experience, this job is more daunting. Amongst the equipment we purchased for acceptance testing and commissioning of the linac were IBA 1D and 2D water phantoms, several ionization chambers, Standard Imaging Electrometer Model CDX2000B, Fluke Biomedical survey meter Model 451P-RYR, IBA MatrixX for monthly quality assurance (QA), Sun Nuclear MapCheck2 IMRT QA device, and Sun Nuclear Daily QA2 for daily output and profile measurements, radiochromic films, and other smaller devices including solid water as well as Perspex phantom slabs of various thicknesses. The process of getting a medical linac into clinical use follows a logical approach. Firstly, there is the installation and fine turning of the mechanical and radiation properties of the linac to meet certain predefined performance parameters and then collecting radiation treatment planning data and other parameters. These parameters are then used to check the consistency of the performance of the linac on a daily, weekly, monthly and annual basis. After the installation of the linac and performing radiation survey measurements to ensure that radiation shielding was adequate, then acceptance testing was based on the manufacturer's acceptance test document even though the work was carried out by a third party oncology service group.

2.1. Mechanical Tests

Mechanical checks are part of linac commissioning. We performed several mechanical tests including: the coincidence between mechanical and radiation isocenters as determined by gantry, collimator and couch rotations; digital and mechanical readout versus spirit level, crosshair center of rotation; light field versus digital collimator readout; coincidence between optical and mechanical distance indicators at several SSDs; light and radiation field coincidence, and laser positions.

2.2. Dosimetric Measurements

Using a reference chamber, commissioning measurements of the radiation dose distribution were undertaken mostly in the 2D IBA water phantom with its associated scanning ionization chambers. We measured all mandatory and recommended data required for beam commissioning. Relative measurements for photon beams included percentage depth dose (PDD) curves, in-plane and cross-plane beam profiles, as well as wedge profiles in the wedge and none wedge directions for various depths and field sizes between 2 × 2 cm^2 and 40 × 40 cm^2 at a source-to-surface distance (SSD) of 100 cm. We also proceeded to measure relative scatter factors for both open field and wedge or enhanced dynamic wedges. The scatter factors (collimator scatter factors, S_c) and phantom scatter factors, S_p) were measured for various photon fields ranging from 4 × 4 cm^2 and 30 × 30 cm^2. The collimator scatter factors were measured in air while the phantom scatter factors were measured in water at d_{max} at 100 cm SSD. Additionally, dynamic wedge field profiles and wedge factors were measured for angles of 15, 30, 45 and 60 degrees. From the photon PDD curves, we determined essential beam characteristics including photon beam quality specifier PDD_{10} (PDD at 10 cm depth), the surface dose D_0, and depth of dose maximum, d_{max}. Likewise, beam profile specifications included flatness, symmetry, and penumbra. The flatness and symmetry which, define beam uniformity were determined within the central 80% of the full-width-at-half maximum (FWHM) of the processed beam profiles [12–14].

Electron beam characterizations included measurements of PDD curves, beam profiles (in-plane and cross-plane), relative electron cone factors (RCFs), and insert correction factors (ICFs) for various cone sizes at 100 cm SSD. The RCF is defined as the ratio of the dose at d_{max} with standard insert in any applicator to the dose at the same depth, d_{max} with standard insert in a 10 × 10 cm^2 applicator. Electron cone sizes ranged from 6 × 6 cm^2 to 25 × 25 cm^2. Electron field characteristics included electron beam quality specifier R_{50} (depth of 50% dose), d_{max}, the depths of 90% (R_{90}) and 80% (R_{80}) dose levels (often referred to as the therapeutic range) as well as the practical range R_p for electrons.

2.3. Machine Calibration

Absolute calibrations of the photon and electron energies were performed in accordance with the American Association of Physicist in Medicine (AAPM) Task Group (TG) 51 protocol [15]. Using this protocol, the absorbed-dose to water D_w^Q at the point of measurement of a calibrated ion chamber placed under reference conditions is given by:

$$D_w^Q = \mathrm{M} k_Q N_{D,w}^{60Co} \quad (5)$$

Where Q is the beam quality of the clinical photon or electron beam; M is the fully corrected ion chamber reading; $N_{D,w}^{\mathrm{Co}}$ is the absorbed-dose to water calibration factor of an ion chamber; and k_Q is the quality conversion factor, which converts the calibration factor for a ^{60}Co beam to that of a beam of quality Q. Full details of the calibration methodology including the definition of k_Q for electron beams are given in the protocol[15] and are not provided here.

Accurate calibrations of the photon beams and three electron energies (6, 9 and 12 MeV) were checked by irradiating the mailed thermoluminescent dosimeters (TLD) service offered by MD Anderson Cancer Center (MDACC). The mailed program reports the dose detected to the dose reported by our institution, COC. Agreement of the TLD dose ratio to within ±5% is considered a satisfactory check for the dose at d_{max}.

The TLD dosimetry system comprised an acrylic mini-phantom loaded with TLDs. The system is based on TLD-100 (LiF:Mg, Ti) powder package into cylindrical Teflon capsules filled with 20–22 mg of crystal. It is calibrated based on the signal-to-noise conversion established with reference dosimeters in a ^{60}Co beam, using a reference dose of 3.0 Gy. An uncertainty of 1.3% in the dose determination allows for a tolerance of ±5% to be used. For each beam being monitored, a separate system was mailed. Beam output was monitored at the depth of maximum dose, d_{max}, and for each beam setup, the dosimetry system was irradiated to a dose level of 3.0 Gy using a field size of 10 × 10 cm^2 at 100 cm SSD.

3. Results

3.1. Mechanical Checks

Table 1 shows results of various mechanical checks which agreed with specified values.

3.2. Dosimetric Characterizations

Figure 1 shows 6 MV photon PDD curves for field sizes between 2 × 2 cm^2 and 40 × 40 cm^2 measured at 100 cm SSD. The characteristics of the PDD curves for both 6 MV and 18 MV beams for various field sizes are listed in Table 2.

Table 1. *Results of mechanical tests.*

Test/Check	Set position		Recorded/Measured value		Specification	Pass/Fail
I. Digital and mechanical readout vs. spirit level						
A. Gantry	180°		180°		+/- 1°	Pass
	90°		89.9°		+/- 1°	Pass
	0° cw		0°		+/- 1°	Pass
	270°		270.3°		+/- 1°	Pass
	0° ccw		359.9°		+/- 1°	Pass
B. Collimator	0°		359.6°		+/- 1°	Pass
	90°		90°		+/- 1°	Pass
	270°		269.9°		+/- 1°	Pass
II. Crosshair center of rotation	Full rotation of collimator		<< 1 mm		+/- 1 mm	Pass
III. Light field vs digital collimator readout	Set field size		Width	Length		
A. Symmetric jaws	5 cm × 5 cm		5.0 cm	5.0 cm	+/- 2 mm	Pass
	10 cm × 10 cm		10.0 cm	10.0 cm	+/- 2 mm	Pass
	20 cm × 20 cm		20.0 cm	20.1 cm	+/- 2 mm	Pass
	30 cm × 30 cm		30.0 cm	30.1 cm	+/- 2 mm	Pass
B. Asymmetric jaws	Width	Length	Width	Length		
X1	10.0 cm	5.0 cm	9.9 cm	5.0 cm	+/- 2 mm	Pass
X2	10.0 cm	5.0 cm	10.0 cm	5.0 cm	+/- 2 mm	Pass
Y1	10.0 cm	5.0 cm	9.9 cm	5.0 cm	+/- 2 mm	Pass
Y1	10.0 cm	5.0 cm	10.0 cm	5.0 cm	+/- 2 mm	Pass
IV. Optical and mechanical distance indicators						
ODI @	80 cm		79.8 cm		+/- 2 mm	Pass
ODI @	90 cm		89.8 cm		+/- 2 mm	Pass
ODI @	100 cm		100.0 cm		+/- 2 mm	Pass
ODI @	110 cm		110.1 cm		+/- 2 mm	Pass
V. Lasers						
Right			1.0 mm		+/- 2 mm	Pass
Left			1.0 mm		+/- 2 mm	Pass
Sagittal			1.0 mm		+/- 2 mm	Pass
Overhead			1.0 mm		+/- 2 mm	Pass

Table 2. *Characteristics of 6 MV and 18 MV photon percent depth dose (PDD) curves for various fields between 5 × 5 cm^2 and 40 × 40 cm^2.*

Photon fields	D_0 (%)	PDD_5 (%)	PDD_{10} (%)	PDD_{15} (%)	PDD_{20} (%)	d_{max} (cm)
6 MV						
5 × 5 cm^2	48.9	85.0	62.2	46.9	34.0	1.4
10 × 10 cm^2	54.1	86.5	66.2	50.7	37.9	1.4
20 × 20 cm^2	62.4	87.7	69.4	55.0	42.0	1.3
30 × 30 cm^2	68.9	88.4	70.5	57.1	43.6	1.2
40 × 40 cm^2	72.6	88.7	70.1	58.0	44.6	1.2
18 MV						
5 × 5 cm^2	24.9	97.7	79.0	64.0	51.1	3.4
10 × 10 cm^2	34.4	96.5	79.1	65.0	52.9	3.2
20 × 20 cm^2	49.6	95.3	79.6	65.8	54.2	2.5
30 × 30 cm^2	57.9	95.2	77.9	66.5	55.1	2.3
40 × 40 cm^2	62.5	95.1	77.9	66.9	53.9	2.2

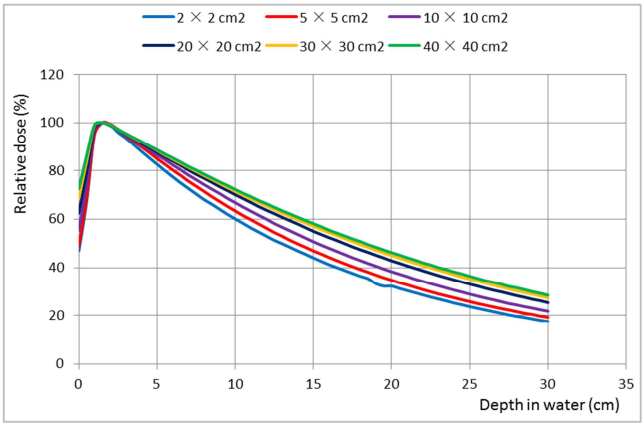

Figure 1. *Percent depth dose curves for various field sizes for the 21EX 6 MV photon beam.*

Figure 2 shows cross-plane 6 MV beam profiles measured at various depths for open fields of 5 × 5 cm^2 and 40 × 40 cm^2 at 100 cm SSD. Displayed in Table 3 are characteristics of both in-plane and cross-plane profiles, which include flatness, symmetry and average penumbra values measured for various 6 MV and 18 MV photon fields at 10 cm depth in water.

Table 3. *Beam profile specifications (flatness, symmetry and average penumbra width) for 6 MV and 18 MV photon beams obtained from measurements of in-plane and cross-plane profiles at 10 cm depth in water for various field sizes at 100 cm SSD.*

Photon fields	Flatness (%)		Symmetry (%)		Average penumbra (±0.01 cm)	
	In-plane	Cross-plane	In-plane	Cross-plane	In-plane	Cross-plane
6 MV						
10 × 10 cm^2	2.7	2.8	1.1	0.5	0.72	0.71
20 × 20 cm^2	--	2.4	--	0.8	--	0.81
30 × 30 cm^2	2.6	1.7	1.0	1.0	0.92	0.92
40 × 40 cm^2	2.3	2.2	1.0	0.8	0.99	0.94
18 MV						
10 × 10 cm^2	2.6	2.6	1.0	0.4	0.84	0.83
20 × 20 cm^2	1.4	1.4	1.1	1.1	0.92	0.89
30 × 30 cm^2	1.4	1.5	0.7	1.0	0.95	0.91
40 × 40 cm^2	1.9	1.8	0.9	0.7	0.96	0.92

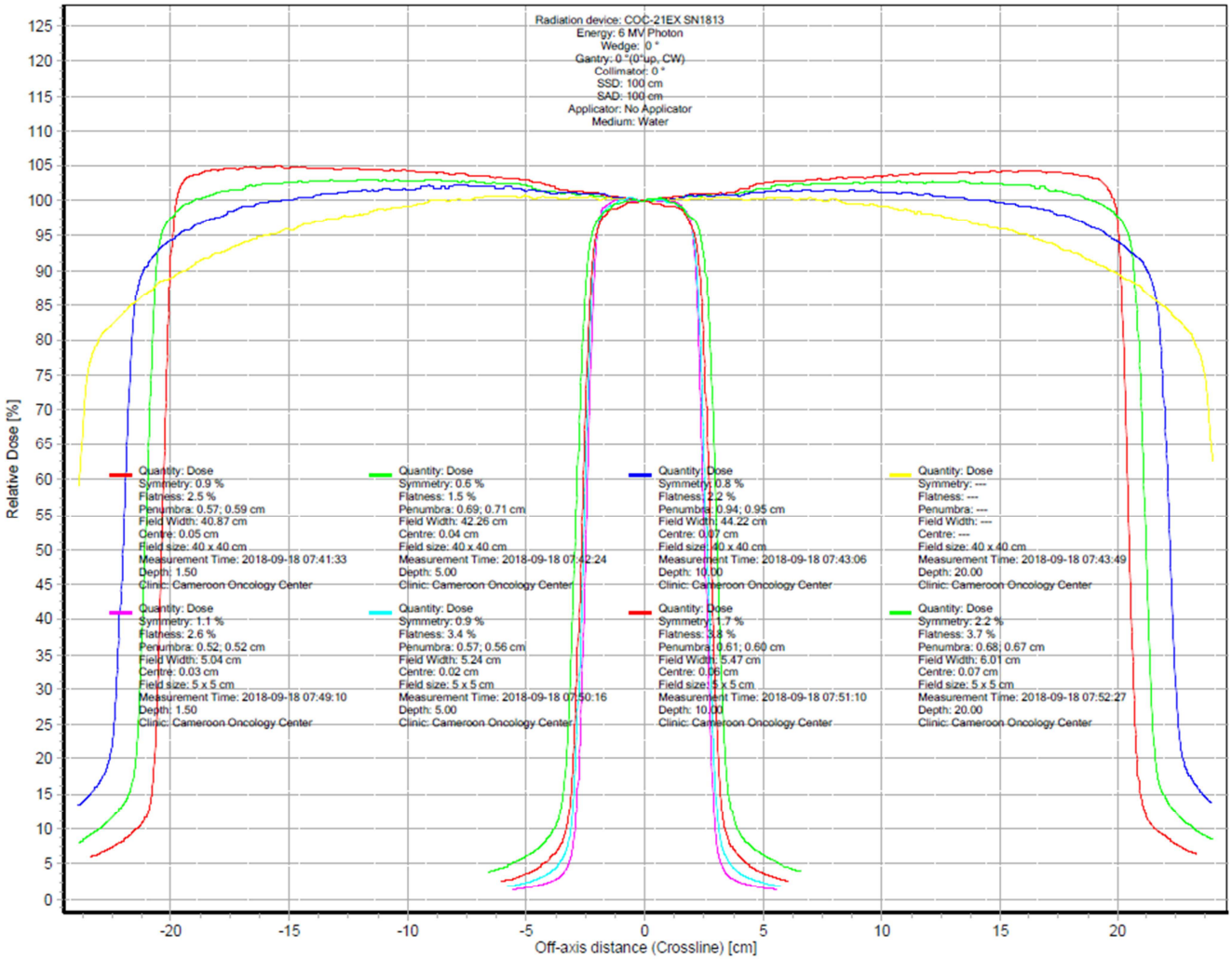

Figure 2. *Cross-plane beam profiles at various depths and fields for the 21EX 6 MV beam.*

Collimator scatter factors ranged from 0.948–1.046 and 0.903–1.067 for 6 MV and 18 MV, respectively. Likewise, phantom scatter factors ranged from 0.981–1.029 for 6 MV and from 0.982–1.024 for 18 MV. As shown in Figure 3 for the 6 MV beam, the relative scatter factors showed increasing trends with field size from 4 × 4 cm^2 to 30 × 30 cm^2.

Figure 4 shows the WTFs measured for a 10 × 10 cm^2 field at d_{max} for various wedge angles. Like in the case for tray factors, the WTF is defined as the ratio of the doses on the beam's central axis in phantom with and without the wedge in place for the same number of monitor units [20].

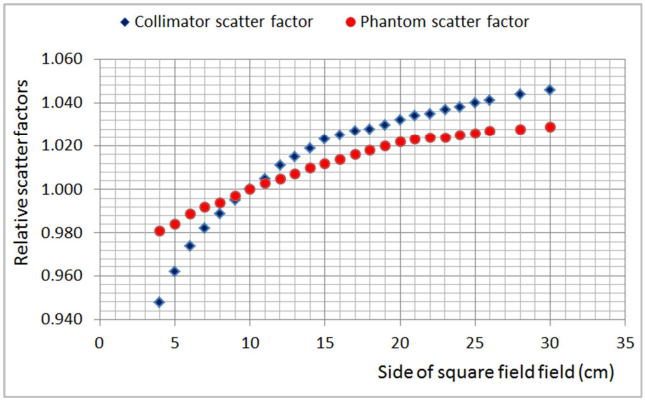

Figure 3. *Variation of relative scatter factors with square field for 6 MV photons.*

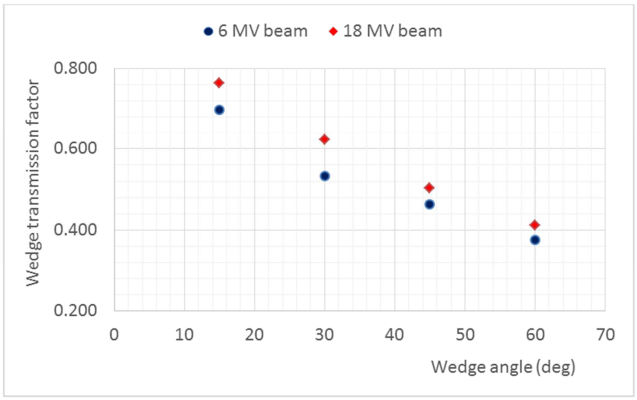

Figure 4. *Wedge transmission factors as a function of wedge angle for 10 × 10 cm² 6 MV and 18 MV beams.*

Figures 5–6 and Tables 4–5 show characteristics of the electron beams. Figure 5 shows electron beam PDD curves for a 10 × 10 cm² applicator-defined field for all the five nominal electron energies. Listed in Table 4 are characteristics of the PDD curves.

Table 4. *Electron percent depth dose characteristics for a 10 × 10 cm² electron field at 100 cm SSD.*

Electron energy (MeV)	d_{max} (cm)	R_{90} (cm)	R_{80} (cm)	R_{50} (cm)	R_p (cm)
6	1.3	1.8	2.0	2.4	3.0
9	2.1	2.8	3.1	3.7	4.5
12	2.8	3.9	4.3	5.1	6.0
16	3.1	5.0	5.6	6.6	8.0
20	2.5	6.0	6.8	8.4	10.0

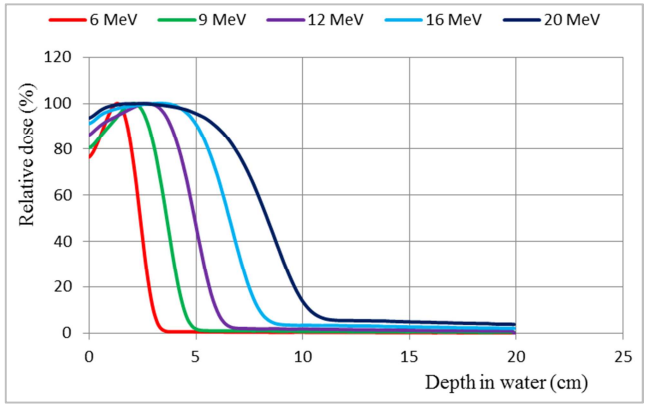

Figure 5. *Percentage depth dose curves for various electron energies measured at 100 cm SSD for a 10 × 10 cm² field.*

Table 5. *Electron beam profile specifications obtained from measurements of in-plane profiles at 2 cm depth in water using applicator sizes of 10 × 10 cm² and 20 × 20 cm².*

Energy (MeV)	Flatness (%)		Symmetry (%)		Average penumbra (±0.01 cm)	
	10 × 10 cm²	20 × 20 cm²	10 × 10 cm²	20 × 20 cm²	10 × 10 cm²	20 × 20 cm²
6	---	2.2	---	1.4	---	1.45
9	4.3	0.9	3.1	0.8	1.15	1.20
12	3.0	0.8	0.4	1.0	0.86	0.87
16	2.1	0.4	1.4	0.5	0.69	0.67
20	1.9	1.2	1.6	0.7	0.59	0.57

Shown in Figure 6 are in-plane profiles measured for a 10 × 10 cm² 16 MeV electron beam at various depths between 2 cm and 6 cm in water. The characteristics of the profiles including flatness, symmetry and average penumbra values measured at depths of 2 cm and 3 cm for 10 × 10 cm² and 20 × 20 cm² applicators are tabulated in Table 5.

The relative electron cone factors for the electron energies for various cone sizes between 6 × 6 cm² and 25 × 25 cm² ranged from 0.971–0.988, 0.988–0.956, 0.988–0.931, 0.966–0.937, and 1.012–0.920, for 6, 9, 12, 16 and 20 MeV, respectively. The cone factors increased with cone size and then decreased again except for the highest 20 MeV electron energy where the cone factors decreased with cone size.

3.3. Machine Calibration

For each photon, and electron energy the 21EX linac was calibrated to deliver nominal 1.0 Gy per 100 MU. In Table 6, the output of the linac at d_{max} for photon and electron beams for the TLD measurements made by the MDACC is compared with dose values reported by COC. It is seen that the results met the MDACC criteria within 3%.

Table 6. *Results of TLD irradiation for monitoring the output of photon, and electron beams at the depth of maximum dose, d_{max}.*

Beam energy	Absorbed radiation dose to water (Gy)		Ratio of MDACC to COC (MDACC/COC)
	Delivered by COC	Measured by MDACC	
6 MV photons	3.0	2.90	0.97
18 MV photons	3.0	2.90	0.97
6 MeV electrons	3.0	3.02	1.01
9 MeV electrons	3.0	2.95	0.98
12 MeV electrons	3.0	2.96	0.99

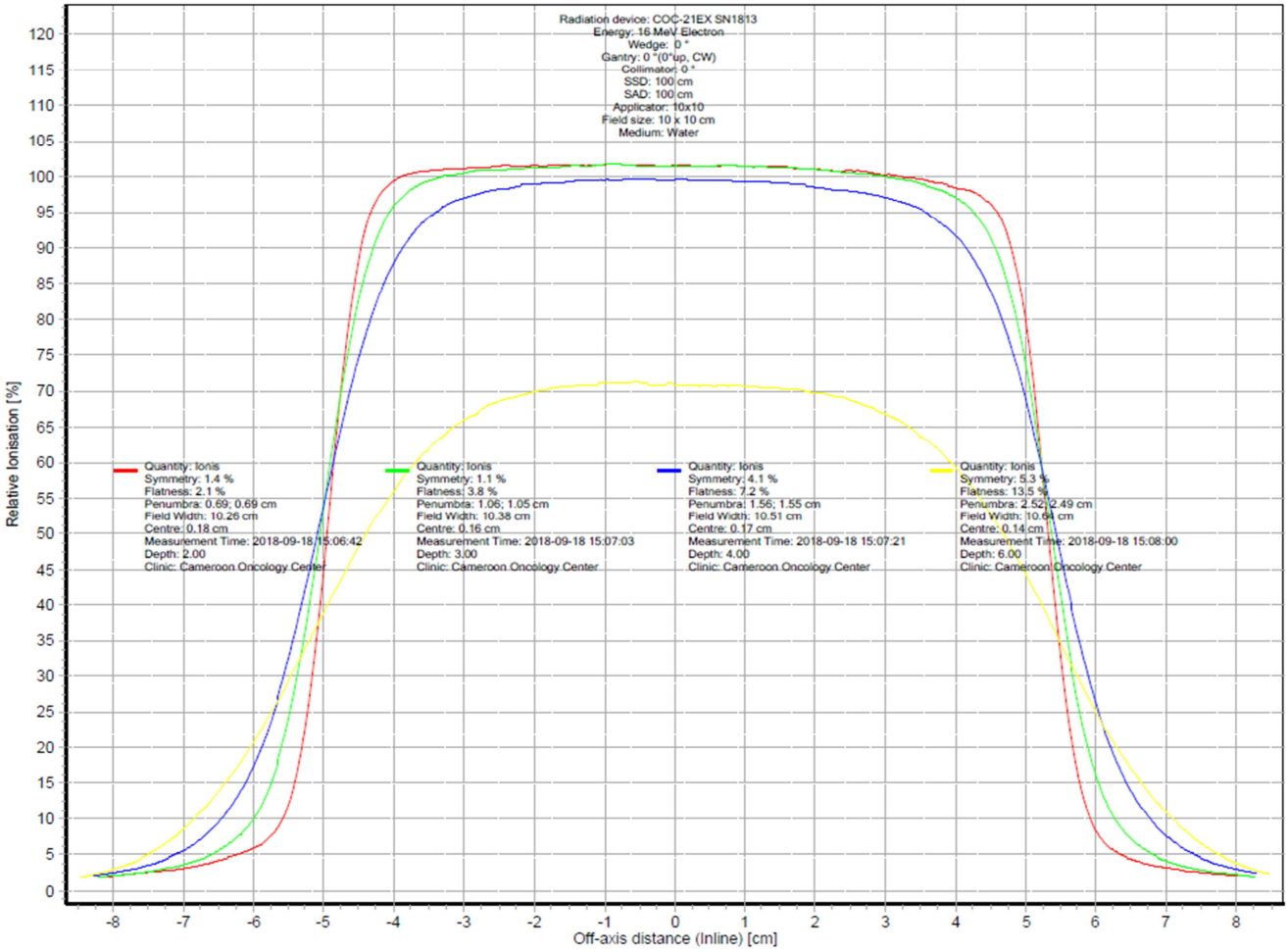

Figure 6. *In-plane beam profiles for a 10 × 10 cm^2 16 MeV electron beam at various depths.*

4. Discussion

This work presents commissioning data for a Varian Clinac 21EX linac installed at Cameroon Oncology Center, a resource-constrained oncology centre in Central Africa. After performing various mechanical checks (Table 1), we proceeded to measure all photon and electron data required for the calculation of machine MU and commissioning of our TPS. The characteristics of photon PDD curves presented in Table 2 show that for each photon beam: (i) the PDDs at various depths including the surface dose D_0 and the beam quality specifier PPD_{10} increase with increase in field size; and (ii) d_{max} decreases with increasing field size. The decrease in d_{max} with increase in radiation field size could be attributed to an increase in electron contamination from the linac head, which raises the surface dose resulting to a shift in d_{max} toward the surface of the phantom. The surface dose, as a part of patient quality assurance (QA) in EBRT, is clinically vital because knowledge of the build-up effect can facilitate preservation of skin sparing or the delivery of an adequate dose to superficial tumours [16]. The severity of skin reactions depends on the radiation dose, energy, as well as the surface area of the skin/tissue irradiated [17–19]. The data for photon beam profile specifications presented in Table 3 shows that while flatness generally decreases with increasing field size, symmetry remains more or less constant with field size. On the other hand, the average penumbra width shows an increasing trend with field size. The electric field characteristics displayed in Table 4 show strong variations with electron energy but not with field size except for the 20 MeV beam where d_{max} increases from 2.0 cm for a 6 × 6 cm^2 field to 2.5 cm for a 25 ×

25 cm^2 field. Beam profile specifications for the electron energies presented in Table 5 show that whereas flatness and symmetry decrease with increase in field size, penumbra does not change with electron field.

We found that the beam commissioning data presented in this report for the Varian 21EX linac compare favourably with data documented for other Varian linacs [13, 14, 21]. Photon PDDs agreed within 1% of the average of several linacs of the same type at depths between 5 and 20 cm, which are consistent with the data used by the manufacturer for acceptance testing. For electrons, the agreement was within 2 mm for R_{50}, R_{90}, R_p, and d_{max}. Symmetry and flatness for all photon and electron beams were within 2% for various fields. All absolute calibrations met the MD Anderson Cancer Center criteria within 3% (Table 6). Therefore, a radiotherapy program based on linac technology has been successfully commissioned in Cameroon for the delivery of high-quality radiation treatments to cancer patients in Central Africa.

5. Conclusion

This work summarizes the commissioning experience of Cameroon's first medical linac. The commissioning data agreed with other linacs of the same type. Moreover, absolute calibrations of the photon and electron energies met the MD Anderson Cancer Center criteria. The commissioning process provided us with data for the calculation of machine monitor units, and for the commissioning of our TPS. Also, we used the commissioning data to establish baseline values for future QA to ensure that the characteristics of the machine do not change from the baselines acquired during the commissioning. As the medical linac is the first of its kind in Central Africa, the commissioning data can provide comparison data to other medical linacs of the same type in the sub-region in the future.

References

[1] Organization and training in radiotherapy for developing countries in Africa. (1991). IAEA-TECDOC-614, IAEA, Vienna.

[2] IAEA International Atomic Energy Agency. (2008). Setting up a radiotherapy program: clinical, medical physics, radiation protection and safety aspect. IAEA, Vienna.

[3] Ferlay, J., Ervik, M., Lam, F., et al., eds. (2020) Global Cancer Observatory: Cancer Today. International Agency for Research on Cancer. https://gco.iarc.fr/today. Accessed June 30, 2021.

[4] Soerjomataram, I., & Bray, F. (2021). Planning for tomorrow: global cancer incidence and the role of prevention 2020–2070. Nat Rev Clin Oncol, 18 (10), 663–672.

[5] IAEA International Atomic Energy Agency. (2016) Accuracy Requirements and Uncertainties in Radiotherapy, IAEA Human Health Series No. 31. IAEA, Vienna.

[6] IARC, World Health Organization International Agency for Research on Cancer. (2021). GLOBOCAN 2020: Estimated cancer incidence, mortality and prevalence worldwide in 2020. https://gco.iarc.fr/today/fact-sheets-populations. Accessed 13 July 2021.

[7] Sung, H., Ferlay, J., & Siegel, R. L. (2021). Laversanne M, Soerjomataram I, Jemel A, Bray F. Global Can Statistics 2020: Globocan estimates of incidence and mortality for 36 cancers in 185 countries. CA Cancer J Clin, 71 (3), 209–249.

[8] Ferlay, J, Ervik M, Lam F, et al. (2018). Cancer today: data visualization tools for exploring the global cancer burden in 2020. Lyon, France: IARC. https://gco.iarc.fr/today.

[9] WHO World Health Organization. (2020). WHO report on cancer: setting priorities, investing wisely and providing care for all. WHO.

[10] Abdel-Wahab, M., Bourque, J. M., Pynda, Y., Iżewska, J., Van der Merwe, D., Zubizarreta, E., & Eduardo, R. (2013). Status of radiotherapy resources in Africa: an International Atomic Energy Agency analysis. Lancet Oncol, 14, e168–e175.

[11] Yao, Q., Zou, L., Lan, H., Luo, S., Lu, S., Lang, J., & Xu, C. (2020). Initial experience of a tele-radiotherapy system for training radiation oncologists in rural areas. J Canc Educ. doi: 10.1007/s13187-020-01836-9.

[12] Podgorsak, E. B. (2005). Radiation Oncology Physics: A handbook for teachers and students. IAEA Vienna.

[13] Gao, S., Balter, P. A., Rose, M., & Simon, W. E. (2016). A comparison of methods for monitoring photon beam energy constancy. J Appl Clin Med Phys, 17 (6), 242–53.

[14] Lloyd, S. A. M., Zavgorodni, S., & Gagne, I. M. (2015). Comparison of measured Varian Clinac 21EX and TrueBeam accelerator electron field characteristics. J Appl Clin Med Phys, 16 (4), 193–201.

[15] Almond, P. R., Biggs, P. J., Coursey, B. M., Hanson, W. F., Huq, M. S., Nath, R., & Rogers, D. W. (1999). AAPM's TG-51 protocol for clinical reference dosimetry of high-energy photon and electron beams. Med Phys, 26 (9), 1847–70.

[16] Wang, Y., Khan, M. K., Ting, J. Y., & Easterling, S. B. (2012). Surface Dose Investigation of the Flattening Filter-Free Photon Beams. Int J Radiation Oncol Biol Phys, 83 (2), e281–e285.

[17] Sun, L. M., Huang, C. J., Chen, H. Y, et al. (2016). Evaluating the consistency of location of the most severe acute skin reaction and highest skin dose measured by thermoluminescent dosimeter during radiotherapy for breast cancer. Med Dosim, 41 (3), 216–20.

[18] McDermott, P. N. (2020). Surface dose and acute skin reactions in external beam breast radiotherapy. Med Dosim, 45 (2), 153–158.

[19] Lee, N., Chuang, C., Quivery, J. M., et al. (2002). Skin toxicity due to intensity modulated radiotherapy for head-and-neck carcinoma. Int J Radiat Oncol Biol Phys, 53 (3), 630–637.

[20] Van Kleffens, H., Venselaar, J., Heukelom, S., Jager, N., Mijnheer, B., van der Laarse, R., van Gasteren, H., & Westermann, C. (1999). Dependence of the tray transmission factor on the collimator setting in high-energy photon beams. Med Phys, 27 (9), 2117–2123.

[21] Glide-Hurst, C., Bellon, M., Foster, R., Altunbas, C., Speiser, M., Altman, M. et al. (2013). Commissioning of the Varian TrueBeam linear accelerator: A multi-institutional study. Med Phys, 40 (3), 031719.